


ORIGINAL ARTICLE OPEN ACCESS

Profiling of RBM20-Regulated CaMKII δ Splice Variants Across the Heart, Skeletal Muscle, and Olfactory Bulbs

Yui Maeda¹ | Yuri Yamasu^{1,2} | Hidehito Kuroyanagi¹ ¹Department of Biochemistry, Graduate School of Medicine, University of the Ryukyus, Okinawa, Japan | ²Life Science and Technology Track, Graduate School of Medical and Dental Sciences, Institute of Science Tokyo, Tokyo, Japan**Correspondence:** Hidehito Kuroyanagi (hidehito@cs.u-ryukyu.ac.jp)**Received:** 27 February 2025 | **Revised:** 28 March 2025 | **Accepted:** 31 March 2025**Transmitting Editor:** Mikiko C Siomi**Funding:** This study was supported by MEXT/JSPS Grant-in-Aid for Scientific Research KAKENHI (JP20K21385 and JP23K18221 to H.K.) and grants from Takeda Science Foundation (to H.K.). This work was also supported by technical training from JSPS KAKENHI Grant Number JP22H04925 (PAGS).**Keywords:** alternative splicing | CaMKII δ | dilated cardiomyopathy | long-read sequencing | RBM20

ABSTRACT

Calcium/calmodulin-dependent protein kinase II δ (CaMKII δ), encoded by the *Camk2d* gene, plays key regulatory roles in various Ca²⁺-regulated cellular processes. Extensive alternative splicing of the *Camk2d* gene generates multiple CaMKII δ splice variants that exhibit differential roles. Despite significant advances in understanding the functions of CaMKII δ , the full repertoire of *Camk2d* splice variants in a variety of tissues and their distinct roles in physiological and pathological contexts remain incompletely characterized due to the complex nature of multiple alternative splicing events. Here, we conducted long-read amplicon sequencing to investigate the murine *Camk2d* splice variants in the heart, skeletal muscle, and olfactory bulbs and show that mRNAs in the heart and skeletal muscle have shorter 3'UTRs. Our results in this study suggest that a key regulator of *Camk2d* splicing, RNA-binding motif protein 20 (RBM20), whose *gain-of-function* mutations cause dilated cardiomyopathy, is crucial for the expression of heart-specific splice variants. Olfactory bulbs specifically express novel splice variants that utilize a mutually exclusive exon 6B and/or an alternative polyadenylation site in a novel exon 17.5 in an RBM20-independent manner. The tissue-specific repertoire of CaMKII δ splice variants and their aberrant expression in disease model animals will help in understanding their roles in physiological and pathological contexts.

1 | Introduction

Calcium/calmodulin-dependent protein kinase II (CaMKII) is a serine/threonine kinase that plays a crucial regulatory role in various Ca²⁺-dependent cellular processes, including excitation–contraction coupling, synaptic plasticity, and gene transcription (Hudmon and Schulman 2002). The CaMKII family is highly conserved among mammalian species and comprises four major enzymatic isoforms (CaMKII α , β , γ , and δ), each encoded by distinct genes and exhibiting tissue-specific expression patterns (Bayer and Schulman 2019). Among these, CaMKII δ ,

encoded by the *Camk2d* gene, is particularly abundant in cardiac and vascular tissues, where it plays a pivotal role in cardiovascular function and pathological remodeling (Anderson et al. 2011).

Alternative splicing of *Camk2d* generates multiple CaMKII δ splice variants with distinct subcellular localization, substrate specificity, and functional properties (Duran et al. 2021; Gray and Heller Brown 2014). In cardiac tissue, predominant splice variants include CaMKII δ_A , δ_C , δ_B , and δ_9 , each contributing uniquely to cardiac physiology and pathology. For instance,

This is an open access article under the terms of the [Creative Commons Attribution-NonCommercial-NoDerivs](https://creativecommons.org/licenses/by-nc-nd/4.0/) License, which permits use and distribution in any medium, provided the original work is properly cited, the use is non-commercial and no modifications or adaptations are made.

© 2025 The Author(s). *Genes to Cells* published by Molecular Biology Society of Japan and John Wiley & Sons Australia, Ltd.

CaMKII δ_A , also known as CaMKII δ_1 , has been implicated in cardiac hypercontractility in conditional *Srsf1* knockout mice (Xu et al. 2005) and in isoproterenol-treated rats (Li, Cai, et al. 2011). CaMKII δ_C , also known as CaMKII δ_2 , has been associated with adverse effects in cardiomyocytes following in vivo ischemia/reperfusion injury (Gray et al. 2017) and pressure overload (Ljubojevic-Holzer et al. 2020). CaMKII δ_B , also known as CaMKII δ_3 , uniquely contains a nuclear localization signal (NLS) encoded by exon 14, leading to its predominant nuclear localization (Srinivasan et al. 1994). Transgenic overexpression of this cardiac-specific isoform induces cardiac hypertrophy (Zhang et al. 2002) but provides protection against ischemia/reperfusion injury (Gray et al. 2017). In contrast, cardiac-specific transgenic overexpression of CaMKII δ_9 results in cardiac hypertrophy, ventricular dilation, and cardiomyocyte death, ultimately progressing to severe heart failure (Zhang et al. 2019).

The alternative splicing of *Camk2d* is regulated in vivo by several RNA-binding proteins (RBPs), including serine/arginine-rich splicing factor 1 (SRSF1, also known as ASF/SF2) (Xu et al. 2005), RNA-binding motif protein 20 (RBM20) (Guo et al. 2012), RNA-binding Fox-1 homolog 2 (RBFOX2) (Wei et al. 2015), and RNA-binding motif protein 24 (RBM24) (Liu et al. 2022). Among these, RBM20 has garnered particular attention due to its strong association with an autosomal dominant form of familial dilated cardiomyopathy (DCM) (Brauch et al. 2009). Pathogenic *RBM20* mutations in familial DCM cases are highly enriched in a five-residue stretch RSRSP, which is essential for RBM20 nuclear localization (Murayama et al. 2018; Watanabe et al. 2018). These missense mutations function in a *gain-of-function* manner, as knock-in mice harboring patient-mimicking mutations exhibit DCM-like phenotypes, whereas knockout mice do not (Ihara et al. 2020; Methawasin et al. 2014; van den Hoogenhof et al. 2018). RNA sequencing (RNA-seq) analysis of human-induced pluripotent stem cell-derived cardiomyocytes (iPSC-CMs) carrying an RSRSP motif mutation revealed aberrant alternative splicing patterns distinct from those observed in RBM20 knockout models (Fenix et al. 2021), suggesting a pathogenic role of splicing dysregulation in DCM. Recently, novel *RBM20* mutations located outside the RSRSP motif have been identified in familial DCM cases (Beqqali et al. 2016; Gaertner et al. 2020), but their effects on RBM20-mediated splicing regulation and DCM pathogenesis remain unexplored in animal models.

Beyond cardiac tissue, CaMKII δ is also expressed in other tissues, including the brain (Sloutsky et al. 2020), skeletal muscle (Eigler et al. 2021), and vascular smooth muscle cells (Li, Li, et al. 2011). Despite significant advances in understanding the function of CaMKII δ , the full repertoire of *Camk2d* splice variants across various tissues and their distinct physiological and pathological roles remains incompletely characterized. In this study, we systematically investigate the diversity of *Camk2d* splice variants in murine heart (ventricles), skeletal muscle (soleus), and olfactory bulbs, a part of the brain. Furthermore, we assess the impact of an established DCM-associated *Rbm20* mutation (S637A, substituting the first serine residue in the RSRSP stretch) (Ihara et al. 2020) and a novel variant (V894A), which mimics the familial DCM mutation V914A (Gaertner et al. 2020), on *Camk2d* alternative splicing.

2 | Results

2.1 | *Rbm20* Is Expressed in Ventricles, Soleus, and Olfactory Bulbs

To determine whether the *Rbm20* gene is expressed in the soleus and olfactory bulbs in addition to the heart, we performed RT-PCR analysis using RNA extracted from these tissues. As our study focused on the effects of *Rbm20* mutations on *Camk2d* splicing, we utilized wild-type (WT), *Rbm20*^{KO/KO}, *Rbm20*^{S637A/S637A}, and *Rbm20*^{V894A/V894A} mice. RT-PCR revealed that *Rbm20* is expressed in both the soleus and olfactory bulbs, albeit at lower levels compared to the ventricles (Figure 1). We also performed RT-qPCR analysis of the *Rbm20* transcript in the wild-type tissues. According to the $\Delta\Delta C_T$ method with the *Gapdh* gene as an internal control, *Rbm20* expression in the soleus and olfactory bulbs was lower than in ventricles by > 25-fold ($\Delta\Delta C_T = 4.83$) and > 8-fold ($\Delta\Delta C_T = 3.11$), respectively (Supp. Figure 1).

2.2 | Multiple *Camk2d* Variants Are Expressed in Ventricles, Soleus, and Olfactory Bulbs

The Reference Sequence (RefSeq) database (release 227, NCBI) (O'Leary et al. 2016) lists nine splice variants of the murine *Camk2d* gene, including previously uncharacterized exons (see Figure 2). The RefSeq sequences NM_001025439 and NM_001346636 contain an exon located downstream of, and homologous to, exon 6. Given that these exons were mutually exclusive in our experiments, we designated them as exons 6A and 6B (Figure 2A). Additionally, NM_001293666 ends with a novel long and polyadenylated exon (2732bp) situated between exons 17 and 18, which we termed exon 17.5. This exon contains a termination codon and five putative polyadenylation signals (PASs, AATAAA) (Figure 2A). Exon 21, which also harbors a termination codon, is a cassette exon (Figure 3), and its skipping results in alternative C-terminal sequences for CaMKII δ (Duran et al. 2021). The longest and last exon (3569bp) in other RefSeq sequences, exon 22, contains eight putative PASs (Figure 2A),

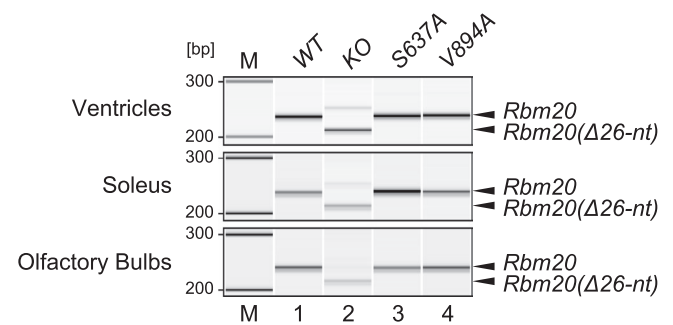


FIGURE 1 | Expression of *Rbm20* in ventricles, soleus, and olfactory bulbs. RT-PCR analysis of *Rbm20* transcripts in ventricles (top), soleus (middle), and olfactory bulbs (bottom) from 8- to 9-week-old wild-type (lane 1), *Rbm20*^{KO/KO} (lane 2), *Rbm20*^{S637A/S637A} (lane 3), and *Rbm20*^{V894A/V894A} (lane 4) mice. Note that the RT-PCR products from *Rbm20*^{KO/KO} tissues (212 bp) were shorter than those from the other genotypes (238 bp) due to 26-nucleotide (nt) deletion within the amplicon. M, DNA1000 ladder. Bioanalyzer-generated gel-like images (Agilent) are shown.

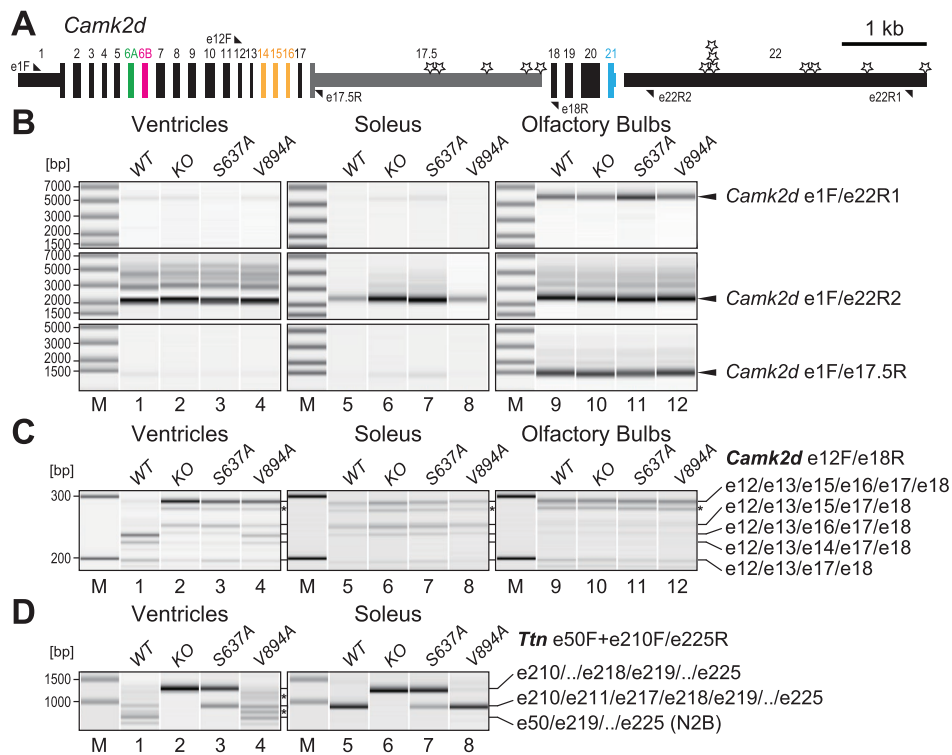


FIGURE 2 | Expression of *Camk2d* isoforms in ventricles, soleus, and olfactory bulbs. (A) Schematic representation of the *Camk2d* gene structure. Exons are represented as boxes, with untranslated regions (UTRs) depicted as thinner boxes. Alternative exons are colored. Triangles indicate the positions of primers used in (B) and (C). Stars denote putative PASs (AATAAA). Introns are not scaled. Note that exon 17.5 and exon 22 are mutually exclusive last exons and never co-included. (B) RT-PCR analysis of *Camk2d* mRNAs in ventricles (lanes 1–4), soleus (lanes 5–8), and olfactory bulbs (lanes 9–12) from 8- to 9-week-old wild-type (lanes 1, 5, 9), *Rbm20*^{KO/KO} (lanes 2, 6, 10), *Rbm20*^{S637A/S637A} (lane 3, 7, 11), and *Rbm20*^{V894A/V894A} (lane 4, 8, 12) mice. Top: RT-PCR using primers e1F/e22R1 (specific to exon 22 isoforms with the longest 3'UTR). Middle: Primers e1F/e22R2 (detecting all exon 22 isoforms). Bottom: Primers e1F/e17.5R (specific to exon 17.5 isoforms). (C, D) RT-PCR analysis of *Camk2d* mRNAs with primers e12F/e18R (C) and *Ttn* mRNAs with primers e50F + e210F/e225R (D). Templates are prepared as in (B). ./ indicates that all exons between these exons are included. N2B is a heart-specific and RBM20-dependent *Ttn* isoform. Asterisks denote artificial PCR products due to the presence of multiple amplicons. Bioanalyzer-generated gel-like images (Agilent) are shown. M, DNA ladder. Identity of the bands were determined by (1) their size estimated by Bioanalyzer, (2) cloning and/or Sanger sequencing, and (3) long-read amplicon sequencing in this study.

suggesting the presence of mRNAs with shorter 3' untranslated regions (3'UTRs).

To verify the expression of these novel variants across tissues, we designed reverse primers targeting specific exon-polyadenylation site combinations. Primer e22R1 selectively amplified mRNAs with the longest 3'UTR, while e22R2 amplified all exon 22-containing mRNAs (Figure 2A). We also designed e17.5R to detect mRNAs that end with exon 17.5.

RT-PCR analysis revealed that *Camk2d* transcripts with the longest 3'UTR were readily detected in the olfactory bulbs but not in the ventricles or soleus (Figure 2B, top panels), even though shorter 3'UTR-containing mRNAs were present in all tissues (Figure 2B, middle panels). Similarly, mRNAs ending with exon 17.5 were detected predominantly in the olfactory bulbs (Figure 2B, bottom panels). Importantly, the use of these alternative polyadenylation sites was not qualitatively altered by any of the *Rbm20* mutations (Figure 2B), suggesting that the selection among multiple PASs occurs in a tissue-specific, but RBM20-independent, manner.

To further investigate well-characterized *Camk2d* alternative splicing events involving exons 14–16, we performed RT-PCR using primers e12F and e18R (Figure 2C). Multiple RT-PCR

products were detected in all tissues, although the relative abundance of each splice variant in the wild-type mouse was different in the soleus and olfactory bulbs compared to that in the ventricles. We confirmed RBM20-dependent regulation of these exons in the ventricles (Figure 2C, lanes 1–4), consistent with our previous findings (Ihara et al. 2020; Murayama et al. 2018). Notably, the splicing patterns in the soleus and olfactory bulbs were apparently unaffected in any of the *Rbm20* mutant mice (Figure 2C, lanes 5–12). To ask if the low level of RBM20 is functional in the soleus, we also analyzed alternative splicing patterns of *Ttn*, a major target for splicing regulation by RBM20 in the heart. We found that skipping of *Ttn* exons 212–216 is fully dependent on RBM20 in both ventricles (Figure 2D, lanes 1–4) and soleus (lanes 5–8). These results indicate that multiple *Camk2d* splice variants are expressed in a tissue-specific manner and that some of them are regulated by RBM20 in the ventricles.

2.3 | Long-Read Sequencing Reveals Exon Composition and Expression Levels of *Camk2d* Splice Variants

To systematically analyze the repertoire of *Camk2d* isoforms expressed in excitable tissues, we performed high-throughput

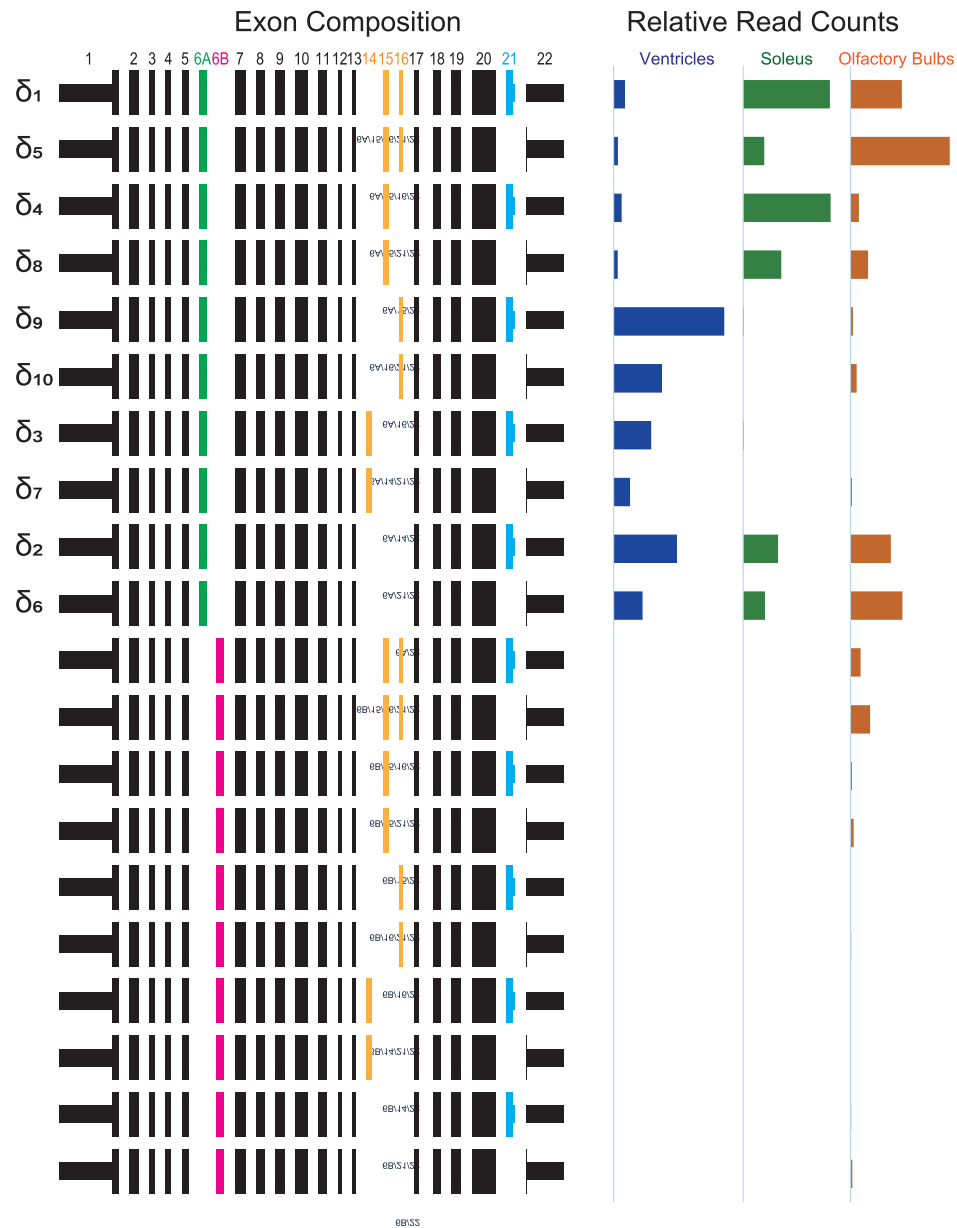


FIGURE 3 | Long-read sequencing of *Camk2d* splice variants with a long exon-22 3'UTR expressed in a wild-type mouse. Left: Schematic representation of *Camk2d* splice variants. Alternative exons are colored. Right: Relative read counts of cDNA amplicons (e1F/e22R2) from wild-type ventricles (1641 reads), soleus (360 reads), and olfactory bulbs (2615 reads). Variants are categorized based on exon 6A/6B selection. Isoforms with frequencies <1% were omitted. Note that the cassette exons 14, 15, and 16 are multiple of three base pairs in length and their inclusion or skipping do not cause a frameshift.

long-read sequencing of full-length *Camk2d* amplicons obtained from the RT-PCR products in Figure 2B. Libraries were prepared by pooling three RT-PCR products per sample (amplified using e1F/e22R1, e1F/e22R2, and e1F/e17.5R) and barcoding them before sequencing. Twelve samples (from three tissues across four genotypes) were pooled and analyzed on a nanopore sequencing platform. Reads were mapped to classify transcripts based on 48 possible exon combinations.

Analysis of full-length sequencing reads from wild-type ventricles, soleus, and olfactory bulbs revealed tissue-specific exon selection (Figure 3). The ventricles and soleus exclusively selected exon 6A, whereas olfactory bulbs expressed a subset of isoforms containing exon 6B. Alternative splicing patterns

of the CaMKII δ variable linker domain (exons 14–16) also varied across tissues. In ventricles, predominant isoforms included e16-only variants (δ_9 , δ_{10}), e14-only variants ($\delta_{3/B}$, δ_7), and exon 14/15/16-skipped variants ($\delta_{2/C}$, δ_6). These findings are consistent with prior long-read amplicon sequencing of murine *Camk2d* transcripts (Zhang et al. 2019), validating our methodology.

2.4 | RBM20 Regulates Heart-Specific Alternative Splicing of the *Camk2d* Gene

To determine the impact of *Rbm20* mutations on *Camk2d* alternative splicing, we analyzed transcript isoforms in ventricles,

soleus, and olfactory bulbs from *Rbm20*^{KO/KO}, *Rbm20*^{S637A/S637A}, and *Rbm20*^{V894A/V894A} mice (Figure 4).

As expected, *Rbm20* knockout and the S637A mutation drastically altered the proportions of *Camk2d* splice variants in the ventricles (Figure 4A), consistent with the RT-PCR results (Figure 2C). On the other hand, exon 21 is prone to being included in ventricles regardless of the *Rbm20* genotypes, suggesting that exon 21 regulation is independent of RBM20 activity (Figure 4A). The *Rbm20*^{V894A} mutation exhibited a modest effect on RBM20-mediated alternative splicing, indicating a partial *loss-of-function* phenotype for *Camk2d* regulation.

In contrast, *Camk2d* isoform proportions in the soleus (Figure 4B) and olfactory bulbs (Figure 4C) remained largely unaffected by *Rbm20* mutations, despite detectable *Rbm20* expression in these tissues (Figure 1). These findings confirm that RBM20-dependent regulation is specific to the heart, influencing the expression of ventricular-enriched *Camk2d* splice variants, including δ_9 , δ_{10} , $\delta_{3/B}$, and δ_7 .

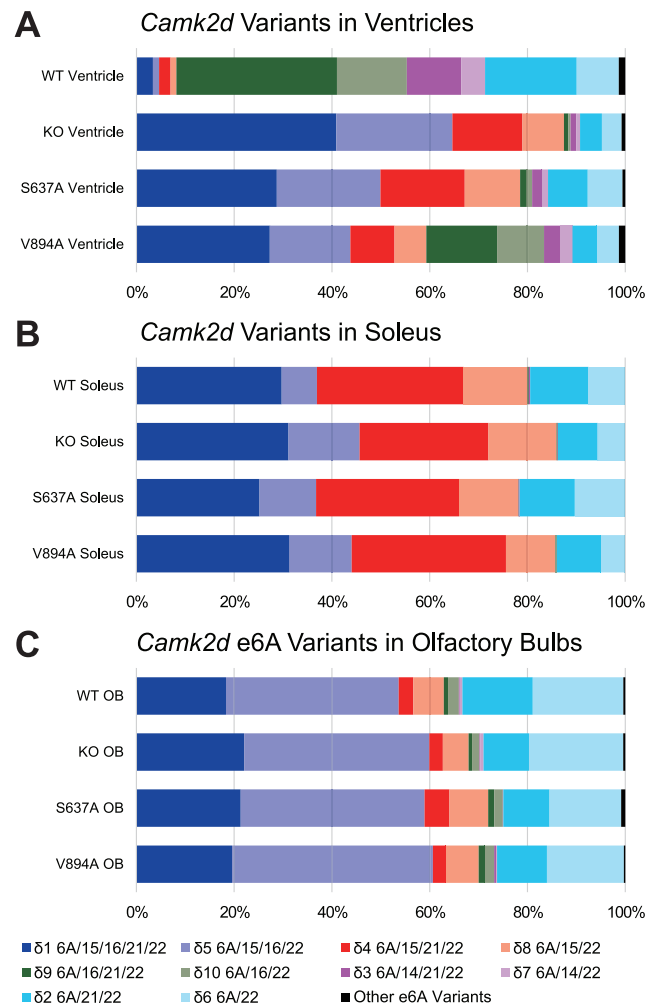


FIGURE 4 | RBM20 regulates heart-specific alternative splicing of *Camk2d*. (A–C) Proportions of *Camk2d* splice variants in ventricles (A), soleus (B), and olfactory bulbs (C) from 8- to 9-week-old animals of the indicated genotypes. Only variants containing exon 6A are shown; other isoforms specific to the olfactory bulbs are analyzed in Figure 5.

2.5 | Olfactory Bulbs Express Unique Splice Variants of the *Camk2d* Gene

To further characterize the unique repertoire of *Camk2d* transcripts in olfactory bulbs, we performed an additional round of long-read amplicon sequencing using RNA from wild-type and *Rbm20* mutant mice (Figure 5).

We obtained full-length sequencing reads from amplicons amplified using e22R1, which selectively targets exon 22-containing transcripts with the longest 3'UTR (Figure 2A). Among these, exon 6B-containing variants accounted for 10.2%–12.4% of total reads, indicating alternative exon 6 selection in a subset of olfactory bulb *Camk2d* mRNAs (Figure 5A, top panel). Alternative splicing patterns of exons 14–16 in these exon 6B variants were similar to those observed for exon 6A variants, though inclusion of exons 15 and 16 was more prevalent (Figure 5A, bottom panel).

To determine whether exon 22 splice variant distributions differed based on 3' UTR length, we analyzed amplicons amplified with e22R2, which detects all exon 22-containing mRNAs. The proportions of splice variants detected using e22R2 (Figure 5B) were highly similar to those obtained using e22R1 (Figure 5A), suggesting that most, if not all, exon 22-containing mRNAs in olfactory bulbs possess the longest 3' UTR.

Additionally, sequencing of exon 17.5-containing variants (amplified using e17.5R) revealed unique alternative splicing patterns in olfactory bulbs. The majority of *Camk2d* mRNAs containing exon 17.5 lacked exons 14, 15, and 16 (Figure 5C). Notably, 4.2%–10.0% of exon 17.5-containing transcripts included exon 6B, with most of these also retaining exons 15 and 16 (Figure 5C).

Importantly, *Rbm20* mutations did not apparently alter the proportions of *Camk2d* transcripts in olfactory bulbs (Figure 5A–C), reinforcing the conclusion that olfactory bulb-specific alternative splicing is independent of RBM20. These results indicate that the olfactory bulbs express a unique set of *Camk2d* isoforms, including mRNAs with the longest 3'UTR, exon 6B variants, and exon 17.5-containing transcripts with distinct C-terminal and 3'UTR structures, none of which are regulated by RBM20.

3 | Discussion

In this study, we conducted long-read amplicon sequencing of *Camk2d* transcripts and demonstrated several key findings: (i) the olfactory bulbs predominantly express mRNAs with the longest 3' UTR, whereas the ventricles and soleus preferentially express mRNAs with shorter 3' UTRs (Figure 2B); (ii) wild-type ventricles express 10 major *Camk2d* splice variants containing exon 6A, consistent with previous reports (Zhang et al. 2019), whereas the soleus expresses only six of these isoforms (Figures 3 and 4A); (iii) expression of four ventricular-specific isoforms is absolutely dependent on RBM20 (Figure 4A); (iv) the olfactory bulbs uniquely express novel *Camk2d* variants containing exons 6B and/or 17.5, in addition to those containing exons 6A and 22 (Figures 3 and 5); and (v) despite detectable *Rbm20* expression in the soleus and olfactory bulbs (Figure 1), the proportions of *Camk2d* splice variants in these tissues remain largely unaffected by *Rbm20* mutations (Figures 4 and 5).

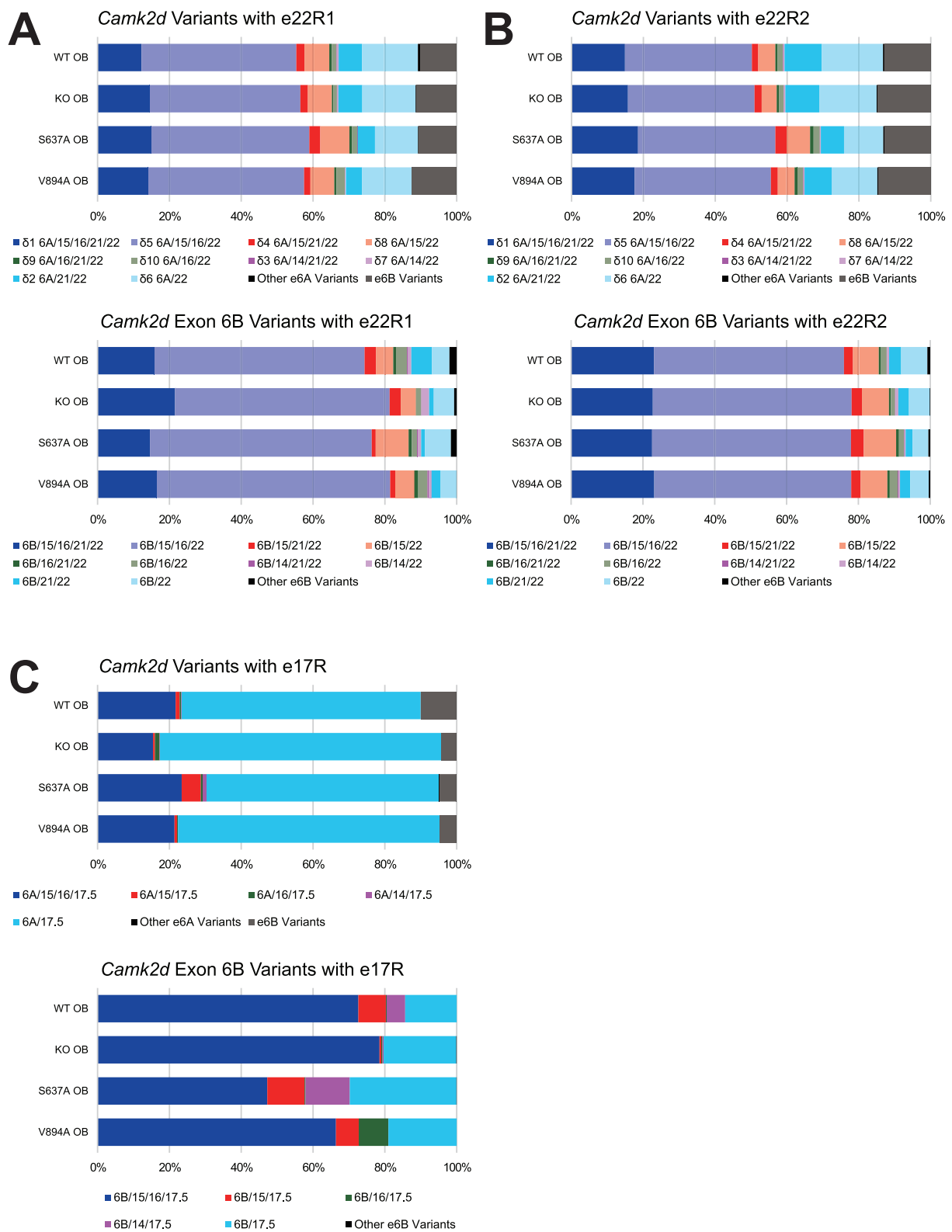


FIGURE 5 | Unique splice variants of *Camk2d* expressed in olfactory bulbs. (A–C) Proportions of *Camk2d* splice variants expressed in olfactory bulbs, amplified using reverse primers e22R1 (A), e22R2 (B), and e17.5R (C) from 8- to 9-week-old animals of the indicated genotypes. Top panels: Proportions of all detected variants. Bottom panels: Proportions of exon 6B-containing variants (gray in Top panels).

Long-read sequencing provided a comprehensive view of *Camk2d* alternative splicing and polyadenylation, revealing distinct selection patterns for each event. Exon 14, which encodes an NLS (Srinivasan et al. 1994), is included exclusively in the

ventricles in an RBM20-dependent manner (Figures 3 and 4). Even with our results, it is still difficult to assign the molecular function of RBM20 to a single alternative splicing event in the *Camk2d* gene. This may be because of RBM20-independent

tight regulation of *Camk2d* splicing. Notably, exon 14 is never co-included with exon 15 or 16, regardless of tissue type or *Rbm20* genotype (Figures 3–5). Interestingly, the low level of RBM20 can still repress *Ttn* exons 212–216 in the soleus (Figure 2D). This may be due to multiple potential binding sites for RBM20 as well as coordinated regulation with other unidentified tissue-specific regulator(s). Exon 21 inclusion and exclusion are observed across all examined tissues (Figure 3). Within each tissue, the ratio of exon 21-included to exon 21-excluded variants appears constant among transcripts with otherwise identical splicing patterns, although this ratio differs among tissues (Figure 4). This observation suggests that exon 21 regulation occurs in a tissue-specific manner, independent of other alternative exons.

Exon 6B is utilized in approximately 10% of *Camk2d* transcripts exclusively in the olfactory bulbs (Figure 5). The presence of exon 6B has also been predicted in the human *CAMK2D* gene based on RefSeq models (O’Leary et al. 2016) and short-read amplicon sequencing (Sloutsky et al. 2020). The amino acid sequences encoded by exons 6A and 6B are highly conserved between humans and mice (Figure 6), suggesting a conserved functional role. The physiological significance of tissue-specific regulation of these mutually exclusive exons remains to be elucidated. The alternative exon 17.5 is also specifically utilized in the olfactory bulbs (Figure 2). Splicing patterns of other *Camk2d* exons in transcripts ending with exon 17.5 differ from those in transcripts ending with exon 22 (Figure 5), suggesting coordinated regulation of upstream exons and alternative polyadenylation at exon 17.5, likely in a neuron-type-specific manner. Given that longer 3’UTRs generated by alternative polyadenylation frequently serve as binding sites for microRNAs (Pereira-Castro and Moreira 2021), *Camk2d* mRNAs in the olfactory bulbs—characterized by the longest 3’UTRs—may be subjected to an additional layer of post-transcriptional regulation via translational control.

The limitation of this study is in the limitation of read numbers of the long-read sequencing. Because we pooled libraries from multiple animals, tissues, and primer pairs for a gene with tens of variants, the number of reads for minor variants is not large enough for statistical analysis. As we have multiple *Rbm20* alleles, we could discuss the effect of *Rbm20* mutations on *Camk2d* splicing.

Gain-of-function mutations within the RSRSP stretch of RBM20, which result in the formation of aberrant cytoplasmic RBM20 condensates, have been strongly associated with DCM in human patients (Schneider et al. 2020) and animal models (Ihara et al. 2020; Kornienko et al. 2023; Nishiyama et al. 2022; Schneider et al. 2020; Wang et al. 2022). In this study, we also

analyzed the effect of the *Rbm20*^{V894A} mutation (Y.Y. and H.K., unpublished) on *Camk2d* splicing and demonstrated that this mutation reduces RBM20 function, at least in terms of *Camk2d* alternative splicing (Figure 4A). Among the RBM20-regulated genes, aberrant *Camk2d* splicing has been proposed as a key contributor to DCM-like phenotypes (Lennermann et al. 2020). However, it remains unclear whether mis-splicing of *Camk2d* or other RBM20 target genes directly contributes to DCM pathology, as altered splicing coincides with the formation of cytoplasmic RBM20 condensates. Notably, pathogenic *RBM20* mutations in human iPSC-CMs (Fenix et al. 2021; Nishiyama et al. 2022; Wyles et al. 2016; Zhu et al. 2021) and a pig model (Schneider et al. 2020) cause widespread alterations in the splicing of over 100 genes associated with cardiac function. Despite these widespread splicing changes, *Camk2d* is one of the few genes consistently affected in murine *Rbm20* knock-in and knockout models (Ihara et al. 2020; Yamamoto et al. 2022).

The detailed analysis of full-length *Camk2d* mRNA isoforms presented in this study provides valuable insights into the role of RBM20 in cardiac splicing regulation. These findings will contribute to future investigations into how pathogenic *Rbm20* mutations affect cardiomyocyte function and potentially influence alternative splicing in other tissues.

4 | Experimental Procedures

4.1 | Animals

All animal experiments were conducted in accordance with the *Guide for the Care and Use of Laboratory Animals* (National Research Council, The National Academies Press, 8th edition, 2011). The study protocol was approved by the Institutional Animal Care and Use Committee of the University of the Ryukyus (Approval Nos. A2021026 and A2024042).

The Generation of the *Rbm20*^{S637A} knock-in allele (Murayama et al. 2018) and the *Rbm20*^{KO} allele (Ihara et al. 2020) has been described previously. The generation of the *Rbm20*^{V894A} knock-in allele will be reported elsewhere (Y.Y. and H.K., unpublished). Briefly, this allele was introduced using a cloning-free CRISPR/Cas system (Aida et al. 2015). A wild-type (WT) mouse strain C57BL/6J was used as a control.

4.2 | RNA Extraction and RT-PCR

Total RNA was extracted from heart ventricular tissues of anesthetized 8- to 9-week-old male mice using the RNeasy Mini Kit (QIAGEN) with on-column DNase I treatment (QIAGEN), following the manufacturer’s protocol for fibrous tissues. Complementary DNA (cDNA) was synthesized from total RNA using the PrimeScript II 1st strand cDNA Synthesis Kit (Takara). The RNA input amounts were as follows: 1.6 µg for ventricles, 0.32 µg for soleus muscle, and 0.24 µg for olfactory bulbs.

Semi-quantitative RT-PCR was performed to analyze alternative splicing patterns using PrimeSTAR GXL DNA Polymerase (Takara) or KOD One PCR Master Mix (TOYOBO). PCR primers were synthesized by Eurofins or Merck, with sequences provided

Human Exon 6A (115>138)	HCIQQILES ^V NHCHLNG ^I TVHRDLK
Mouse Exon 6A (115>138)	HCIQQILES ^V NHCHLNG ^I TVHRDLK
Human Exon 6B (115>138)	HCIQQILEAVLHCHQMG ^V VHRDLK
Mouse Exon 6B (115>138)	HCIQQILEAVLHCHQMG ^V VHRDLK

FIGURE 6 | Evolutionary conservation of CaMKIIδ exon 6A/6B sequences. Amino acid sequence alignment of the CaMKIIδ protein kinase domain encoded by exons 6A and 6B from human and mouse. Identical residues across all sequences are highlighted in black, while residues differing between exons 6A and 6B are shaded in gray. Amino acid positions in each protein are indicated.

in Table S1. PCR products were analyzed using a Bioanalyzer 2100 Expert system with DNA7500 or DNA1000 Kits (Agilent).

Quantitative PCR (qPCR) was performed to determine *Rbm20* expression levels relative to *Gapdh* using TB Green Premix Ex Taq II (Takara) and StepOnePlus Real-Time PCR System (Applied Biosystems), following the manufacturer's standard protocol. PCR primers were synthesized by Eurofins or Merck, with sequences provided in Table S2. The *Rbm20* primers were designed following a previous report (Zhang et al. 2022).

4.3 | Library Preparation and Long-Read Sequencing

Long-range PCR for amplicon sequencing was performed using KOD One PCR Master Mix (TOYOBO) following the manufacturer's step-down protocol. Primer sequences are listed in Table S1.

Nanopore amplicon sequencing libraries were prepared using the Ligation Sequencing Kit V14 (SQK-LSK114) and PCR Barcoding Expansion Pack 1–12 (EXP-PBC001) (Oxford Nanopore Technologies), according to the manufacturer's instructions. Long-read sequencing was performed on a MinION Mk1B platform (Oxford Nanopore Technologies) using Flongle or MinION/ GridION Flow Cells, following the standard protocol.

4.4 | Data Analysis

Raw sequencing reads were processed using default parameters. Transcript isoform analysis was performed using IsoQuant 3.6 (Prjibelski et al. 2023), with *Mus musculus* reference genome data (mm39) obtained from the UCSC Genome Browser (Perez et al. 2025). A custom-prepared annotation file in GTF format was used for mapping *Camk2d* transcripts.

Amino acid sequence alignments of the CaMKII δ protein kinase domain were conducted using the MegAlign Pro module of Lasergene Molecular Biology Ver. 18 (DNASTAR).

Author Contributions

Y.M., Y.Y., and H.K. contributed to molecular and animal experiments. Y.Y. and H.K. contributed to data analysis. H.K. wrote the manuscript.

Acknowledgments

We thank Akiko Ishii and Kuniko Oshiro for their technical assistance in the maintenance of the gene-modified mice. We thank the Institute for Animal Experiments and the Research Laboratory Center of the Faculty of Medicine, and the Research Facility Center of the University of the Ryukyus for supporting our experiments.

Conflicts of Interest

The authors declare no conflicts of interest.

Data Availability Statement

The data that support the findings of this study are available from the corresponding author upon reasonable request.

References

- Aida, T., K. Chiyo, T. Usami, et al. 2015. "Cloning-Free CRISPR/Cas System Facilitates Functional Cassette Knock-In in Mice." *Genome Biology* 16, no. 1: 87. <https://doi.org/10.1186/s13059-015-0653-x>.
- Anderson, M. E., J. H. Brown, and D. M. Bers. 2011. "CaMKII in Myocardial Hypertrophy and Heart Failure." *Journal of Molecular and Cellular Cardiology* 51, no. 4: 468–473. <https://doi.org/10.1016/j.jymcc.2011.01.012>.
- Bayer, K. U., and H. Schulman. 2019. "CaM Kinase: Still Inspiring at 40." *Neuron* 103, no. 3: 380–394. <https://doi.org/10.1016/j.neuron.2019.05.033>.
- Beqqali, A., I. A. Bollen, T. B. Rasmussen, et al. 2016. "A Mutation in the Glutamate-Rich Region of RNA-Binding Motif Protein 20 Causes Dilated Cardiomyopathy Through Missplicing of Titin and Impaired Frank-Starling Mechanism." *Cardiovascular Research* 112, no. 1: 452–463. <https://doi.org/10.1093/cvr/cvw192>.
- Brauch, K. M., M. L. Karst, K. J. Herron, et al. 2009. "Mutations in Ribonucleic Acid Binding Protein Gene Cause Familial Dilated Cardiomyopathy." *Journal of the American College of Cardiology* 54, no. 10: 930–941. <https://doi.org/10.1016/j.jacc.2009.05.038>.
- Duran, J., L. Nickel, M. Estrada, J. Backs, and M. M. G. van den Hoogenhof. 2021. "CaMKII δ Splice Variants in the Healthy and Diseased Heart." *Frontiers in Cell and Development Biology* 9: 644630. <https://doi.org/10.3389/fcell.2021.644630>.
- Eigler, T., G. Zarfati, E. Amzallag, et al. 2021. "ERK1/2 Inhibition Promotes Robust Myotube Growth via CaMKII Activation Resulting in Myoblast-To-Myotube Fusion." *Developmental Cell* 56, no. 24: 3349–3363. <https://doi.org/10.1016/j.devcel.2021.11.022>.
- Fenix, A. M., Y. Miyaoka, A. Bertero, et al. 2021. "Gain-Of-Function Cardiomyopathic Mutations in RBM20 Rewire Splicing Regulation and Re-Distribute Ribonucleoprotein Granules Within Processing Bodies." *Nature Communications* 12, no. 1: 6324. <https://doi.org/10.1038/s41467-021-26623-y>.
- Gaertner, A., B. Klauke, E. Felski, et al. 2020. "Cardiomyopathy-Associated Mutations in the RS Domain Affect Nuclear Localization of RBM20." *Human Mutation* 41, no. 11: 1931–1943. <https://doi.org/10.1002/humu.24096>.
- Gray, C. B., and J. Heller Brown. 2014. "CaMKII δ Subtypes: Localization and Function." *Frontiers in Pharmacology* 5: 15. <https://doi.org/10.3389/fphar.2014.00015>.
- Gray, C. B., T. Suetomi, S. Xiang, et al. 2017. "CaMKII δ Subtypes Differentially Regulate Infarct Formation Following Ex Vivo Myocardial Ischemia/Reperfusion Through NF-kappaB and TNF-Alpha." *Journal of Molecular and Cellular Cardiology* 103: 48–55. <https://doi.org/10.1016/j.jymcc.2017.01.002>.
- Guo, W., S. Schafer, M. L. Greaser, et al. 2012. "RBM20, a Gene for Hereditary Cardiomyopathy, Regulates Titin Splicing." *Nature Medicine* 18, no. 5: 766–773. <https://doi.org/10.1038/nm.2693>.
- Hudmon, A., and H. Schulman. 2002. "Neuronal Ca²⁺/Calmodulin-Dependent Protein Kinase II: The Role of Structure and Autoregulation in Cellular Function." *Annual Review of Biochemistry* 71: 473–510. <https://doi.org/10.1146/annurev.biochem.71.110601.135410>.
- Ihara, K., T. Sasano, Y. Hiraoka, et al. 2020. "A Missense Mutation in the RSRSP Stretch of Rbm20 Causes Dilated Cardiomyopathy and Atrial Fibrillation in Mice." *Scientific Reports* 10, no. 1: 17894. <https://doi.org/10.1038/s41598-020-74800-8>.
- Kornienko, J., M. Rodriguez-Martinez, K. Fenzl, et al. 2023. "Mislocalization of Pathogenic RBM20 Variants in Dilated Cardiomyopathy Is Caused by Loss-Of-Interaction With Transportin-3." *Nature Communications* 14, no. 1: 4312. <https://doi.org/10.1038/s41467-023-39965-6>.

- Lennermann, D., J. Backs, and M. M. G. van den Hoogenhof. 2020. "New Insights in RBM20 Cardiomyopathy." *Current Heart Failure Reports* 17, no. 5: 234–246. <https://doi.org/10.1007/s11897-020-00475-x>.
- Li, C., X. Cai, H. Sun, et al. 2011. "The δ A Isoform of Calmodulin Kinase II Mediates Pathological Cardiac Hypertrophy by Interfering With the HDAC4-MEF2 Signaling Pathway." *Biochemical and Biophysical Research Communications* 409, no. 1: 125–130. <https://doi.org/10.1016/j.bbrc.2011.04.128>.
- Li, W., H. Li, P. N. Sanders, et al. 2011. "The Multifunctional Ca²⁺/Calmodulin-Dependent Kinase II δ (CaMKII δ) Controls Neointima Formation After Carotid Ligation and Vascular Smooth Muscle Cell Proliferation Through Cell Cycle Regulation by p21." *Journal of Biological Chemistry* 286, no. 10: 7990–7999. <https://doi.org/10.1074/jbc.M110.163006>.
- Liu, J., K. Wang, X. Liu, et al. 2022. "RBM24 Controls Cardiac QT Interval Through CaMKII δ Splicing." *Cellular and Molecular Life Sciences* 79, no. 12: 613. <https://doi.org/10.1007/s00018-022-04624-4>.
- Ljubojevic-Holzer, S., A. W. Herren, N. Djalalinac, et al. 2020. "CaMKII δ C Drives Early Adaptive Ca²⁺ Change and Late Eccentric Cardiac Hypertrophy." *Circulation Research* 127, no. 9: 1159–1178. <https://doi.org/10.1161/CIRCRESAHA.120.316947>.
- Methawasin, M., K. R. Hutchinson, E. J. Lee, et al. 2014. "Experimentally Increasing Titin Compliance in a Novel Mouse Model Attenuates the Frank-Starling Mechanism but Has a Beneficial Effect on Diastole." *Circulation* 129, no. 19: 1924–1936. <https://doi.org/10.1161/CIRCULATIONAHA.113.005610>.
- Murayama, R., M. Kimura-Asami, M. Togo-Ohno, et al. 2018. "Phosphorylation of the RSRP Stretch Is Critical for Splicing Regulation by RNA-Binding Motif Protein 20 (RBM20) Through Nuclear Localization." *Scientific Reports* 8, no. 1: 8970. <https://doi.org/10.1038/s41598-018-26624-w>.
- Nishiyama, T., Y. Zhang, M. Cui, et al. 2022. "Precise Genomic Editing of Pathogenic Mutations in RBM20 Rescues Dilated Cardiomyopathy." *Science Translational Medicine* 14, no. 672: eade1633. <https://doi.org/10.1126/scitranslmed.ade1633>.
- O'Leary, N. A., M. W. Wright, J. R. Brister, et al. 2016. "Reference Sequence (RefSeq) Database at NCBI: Current Status, Taxonomic Expansion, and Functional Annotation." *Nucleic Acids Research* 44, no. D1: D733–D745. <https://doi.org/10.1093/nar/gkv1189>.
- Pereira-Castro, I., and A. Moreira. 2021. "On the Function and Relevance of Alternative 3'-UTRs in Gene Expression Regulation." *Wiley Interdisciplinary Reviews: RNA* 12, no. 5: e1653. <https://doi.org/10.1002/wrna.1653>.
- Perez, G., G. P. Barber, A. Benet-Pages, et al. 2025. "The UCSC Genome Browser Database: 2025 Update." *Nucleic Acids Research* 53, no. D1: D1243–D1249. <https://doi.org/10.1093/nar/gkae974>.
- Prijbelski, A. D., A. Mikheenko, A. Joglekar, et al. 2023. "Accurate Isoform Discovery With IsoQuant Using Long Reads." *Nature Biotechnology* 41, no. 7: 915–918. <https://doi.org/10.1038/s41587-022-01565-y>.
- Schneider, J. W., S. Oommen, M. Y. Qureshi, et al. 2020. "Dysregulated Ribonucleoprotein Granules Promote Cardiomyopathy in RBM20 Gene-Edited Pigs." *Nature Medicine* 26, no. 11: 1788–1800. <https://doi.org/10.1038/s41591-020-1087-x>.
- Sloutsky, R., N. Dziedzic, M. J. Dunn, et al. 2020. "Heterogeneity in Human Hippocampal CaMKII Transcripts Reveals Allosteric Hub-Dependent Regulation." *Science Signaling* 13, no. 641. <https://doi.org/10.1126/scisignal.aaz0240>.
- Srinivasan, M., C. F. Edman, and H. Schulman. 1994. "Alternative Splicing Introduces a Nuclear Localization Signal That Targets Multifunctional CaM Kinase to the Nucleus." *Journal of Cell Biology* 126, no. 4: 839–852. <https://doi.org/10.1083/jcb.126.4.839>.
- van den Hoogenhof, M. M. G., A. Beqqali, A. S. Amin, et al. 2018. "RBM20 Mutations Induce an Arrhythmogenic Dilated Cardiomyopathy Related to Disturbed Calcium Handling." *Circulation* 138, no. 13: 1330–1342. <https://doi.org/10.1161/CIRCULATIONAHA.117.031947>.
- Wang, C., Y. Zhang, M. Methawasin, et al. 2022. "RBM20S639G Mutation Is a High Genetic Risk Factor for Premature Death Through RNA-Protein Condensates." *Journal of Molecular and Cellular Cardiology* 165: 115–129. <https://doi.org/10.1016/j.jymcc.2022.01.004>.
- Watanabe, T., A. Kimura, and H. Kuroyanagi. 2018. "Alternative Splicing Regulator RBM20 and Cardiomyopathy." *Frontiers in Molecular Biosciences* 5: 105. <https://doi.org/10.3389/fmolb.2018.00105>.
- Wei, C., J. Qiu, Y. Zhou, et al. 2015. "Repression of the Central Splicing Regulator RBFOX2 Is Functionally Linked to Pressure Overload-Induced Heart Failure." *Cell Reports* 10: 1521–1533. <https://doi.org/10.1016/j.celrep.2015.02.013>.
- Wyles, S. P., X. Li, S. C. Hrstka, et al. 2016. "Modeling Structural and Functional Deficiencies of RBM20 Familial Dilated Cardiomyopathy Using Human Induced Pluripotent Stem Cells." *Human Molecular Genetics* 25, no. 2: 254–265. <https://doi.org/10.1093/hmg/ddv468>.
- Xu, X., D. Yang, J. H. Ding, et al. 2005. "ASF/SF2-Regulated CaMKII δ Alternative Splicing Temporally Reprograms Excitation-Contraction Coupling in Cardiac Muscle." *Cell* 120, no. 1: 59–72. <https://doi.org/10.1016/j.cell.2004.11.036>.
- Yamamoto, T., R. Sano, A. Miura, et al. 2022. "I536T Variant of RBM20 Affects Splicing of Cardiac Structural Proteins That Are Causative for Developing Dilated Cardiomyopathy." *Journal of Molecular Medicine (Berlin, Germany)* 100, no. 12: 1741–1754. <https://doi.org/10.1007/s00109-022-02262-8>.
- Zhang, M., H. Gao, D. Liu, et al. 2019. "CaMKII- δ Promotes Cardiomyopathy Through Disrupting UBE2T-Dependent DNA Repair." *Nature Cell Biology* 21, no. 9: 1152–1163. <https://doi.org/10.1038/s41556-019-0380-8>.
- Zhang, T., E. N. Johnson, Y. Gu, et al. 2002. "The Cardiac-Specific Nuclear δ B Isoform of Ca²⁺/Calmodulin-Dependent Protein Kinase II Induces Hypertrophy and Dilated Cardiomyopathy Associated With Increased Protein Phosphatase 2A Activity." *Journal of Biological Chemistry* 277, no. 2: 1261–1267. <https://doi.org/10.1074/jbc.M108525200>.
- Zhang, Y., C. Wang, M. Sun, et al. 2022. "RBM20 Phosphorylation and Its Role in Nucleocytoplasmic Transport and Cardiac Pathogenesis." *FASEB Journal* 36, no. 5: e22302. <https://doi.org/10.1096/fj.202101811RR>.
- Zhu, C., J. Wu, H. Sun, et al. 2021. "Single-Molecule, Full-Length Transcript Isoform Sequencing Reveals Disease-Associated RNA Isoforms in Cardiomyocytes." *Nature Communications* 12, no. 1: 4203. <https://doi.org/10.1038/s41467-021-24484-z>.

Supporting Information

Additional supporting information can be found online in the Supporting Information section.